Egypt. J. Chem. **Vol. 66**, No. SI: 13 pp. 417 - 436 (2023)

Egyptian Journal of Chemistry

http://ejchem.journals.ekb.eg/

Significance of Heat Source and Activation Energy on MHD Peristaltic Transport of Couple Stress Hyperbolic Tangent Nanofluid through an Inclined Tapered Asymmetric Channel

Alaa J. Abuiyada[a]*, Nabil T. Eldabe[b], Mohamed Y. Abou-zeid[b], Sami M. El Shaboury[a]

[a] *Department of mathematics, Faculty of Science, Ain Shams University, Cairo, Egypt*

[b] *Department of mathematics, Faculty of Education, Ain Shams University, Cairo, Egypt*

Abstract

This study has significant applications in an intra-uterine fluid motion with tiny particles in a non-pregnant uterus, and this situation is vital in inspecting the embryo motion in the uterus. This paper presents the influence of chemical reaction and activation energy on peristaltic flow of MHD hyperbolic tangent nanofluid with heat and mass transfer through a non-Darcy porous medium in an inclined tapered asymmetric channel with different wave forms. Brownian motion, thermophoresis, viscous dissipation, couple stresses, Joule heating, Hall currents, radiation, heat generation/absorption, and thermal diffusion and diffusion thermo effects are involved. The coupled non-linear equations that govern the flow are simplified by using the long wavelength and low Reynolds number approximations. Then, an analytical method called homotopy perturbation method (HPM) have been used to solve the simplified equations. Graphical results are obtained to examine the behaviour of various parameters on the velocity, temperature, and nanoparticle concentration distributions. Graphical representations of heat transfer coefficient, Nusselt number, Sherwood number and entropy generation are sketched. Physical explanations for the results are provided. Findings revealed that Weissenberg number We has a dual behaviour on the velocity, temperature, and nanoparticle concentration profiles. The chemical reaction parameter ξ, activation energy parameter E, and temperature difference parameter ρ_1 enhances the velocity, temperature, and nanoparticle concentration profiles.

Keywords: Peristaltic, nanodluid, couple stress, radiation, hyperbolic tangent fluid, tapered asymmetrc channel, HPM

1. Introduction

Peristalsis is a form of fluid transport that occurs due to the contraction and expansion of extensible tube/channel which produces a progressive waves traveling along the length of tube/channel walls. The word peristaltic is derived from the Greek word "Peristaltikos" which means clasping and compressing. Peristaltic is an inherent property of many tubular organs of the living bodies which plays an important role in transporting the physiological fluids. Peristalsis occurs in many parts of the human and animal bodies including the stomach, gastrointestinal tract, and small intestines. Moreover, swallowing food through the esophagus, the motion of chyme in the gastrointestinal tract, the movement of an ovum in a fallopian tube, the transport of lymph in lymphatic vessels, the passage of bile from the gall bladder to the duodenum, the flow of urine from the kidneys to the bladder, and lymph transport in the lymphatic vessel exhibit peristalsis. Furthermore, peristalsis plays an important role in designing of numerous devices like heart lung machines, dialysis machines and blood pump machines that pump the blood during many biomedical processes. Eldabe et

*Corresponding author e-mail: alaaabuiyada2019@gmail.com.; (Alaa J. Abuiyada).
EJCHEM use only: Received date 02 February 2023; revised date 12 February 2023; accepted date 02 March 2023
DOI: 10.21608/EJCHEM.2023.191413.7553

al. [1] studied wall properties effect on the peristaltic motion of a coupled stress fluid with heat and mass transfer through a porous media. Eldabe et al. [2] investigated the effects of heat and mass transfer on Casson fluid between two co-axial tubes with peristalsis. El-dabe and Abou-Zeid [3] studied the radially varying magnetic field effect on peristaltic motion with heat and mass transfer of a non-Newtonian fluid between two co-axial tubes. Eldabe et al. [4] studied homotopy perturbation approach for Ohmic dissipation and mixed convection effects on non-Newtonian nanofluid flow between two co-axial tubes with peristalsis. Recently, there are many researches that are related to the peristaltic motion with various geometries [5-12].

Activation energy is defined as the lowest quantity of energy to initiate a chemical reaction. The activation energy is acting as a fence that separates two energy states. Once this energy is crossed, the chemical reaction gets started. Many researchers investigated the influence of activation energy on MHD peristaltic flow of non-Newtonian nanofluids with heat and mass transfer in the presence of couple stresses due to its wide applications in medical science. Ellahi et al. [13] studied peristaltic blood flow of couple stress fluid suspended with nanoparticles under the influence of chemical reaction and activation energy. Hayat et al. [14] studied activation energy and non-Darcy resistance in magneto peristalsis of Jeffrey material. Nisar et al. [15] investigated the significance of activation energy in radiative peristaltic transport of Eyring-Powell nanofluid. Hayat et al. [16] studied the nonlinear radiative peristaltic flow of Jeffrey nanofluid with activation energy and modified Darcy's law. Ibrahim et al. [17] studied the the inflence of chemical reaction and activation energy on MHD Bingham nanofluid flow inside a non-Darcy porous medium. Ismael et al. [18] analysed the activation energy and chemical reaction effects on MHD Bingham nanofluid flow through a non-Darcy porous media.

Tangent hyperbolic fluid is a non-Newtonian fluid in which the constitutive equation is valid for low and high shear rates. Many researchers have been studied the flow of tangent hyperbolic fluid under the influence of various effects. Nadeem and Akram [19] investigated magnetohydrodynamic peristaltic flow of a hyperbolic tangent fluid in a vertical asymmetric channel with heat transfer. Nadeem and Akram [20] also analysed the peristaltic transport of a hyperbolic tangent fluid model in an asymmetric Channel. Hayat et al. [21] studied the endoscopic effect in MHD peristaltic activity of hyperbolic tangent nanofluid. Hayat et al. investigated [22] the magnetohydrodynamic effects on peristaltic flow of hyperbolic tangent nanofluid with slip conditions and Joule heating in an inclined channel.

The couple stress fluid is a special type of non-Newtonian fluid feature in which the effects of the particles size are taken into account. The couple stress fluid model plays a significance role in describing some of the non-Newtonian flow properties of blood in arteries. Many studies of non-Newtonian fluids with couple stresses effect have been reported. Homotopy perturbation method for couple stresses effect on MHD peristaltic flow of a non-Newtonian nanofluid investigated by Abou-zeid [23]. Alsaedi et al. [24] investigated the effect of couple stresses on the peristaltic flow through a uniform porous medium. Ismael et al. [25] investigated thermal micropolar and couple stresses effects on peristaltic flow of biviscosity nanofluid through a porous medium. Abuiyada et al. [26] investigated the effects of couple stress, and thermal diffusion and diffusion thermo on a chemically reacting MHD peristaltic transport of Bingham plastic nanofluid.

In the current investigation we discuss the impact of activation energy, couple stresses, and Hall currents of peristaltic flow of MHD hyperbolic tangent nanofluid through a non-Darcy porous medium in an inclined tapered asymmetric channel with heat and mass transfer. The influence of viscous dissipation, Joule heating, radiation, heat generation/absorption, and thermal diffusion and diffusion thermo effects are taken into consideration. Further, Brownian motion and thermophoresis are involved. The coupled non-linear equations governing the flow are simplified by using the long wavelength and low Reynolds number approximations. Then, homotopy perturbation method (HPM) is used to solve the simplified non-linear equations. Graphical results for velocity, temperature, and nanoparticle concentration profiles are sketched for various values of interest parameters. Physical explanations of the obtained results are provided. Furthermore, graphical results of heat

transfer coefficient, entropy generation, Nusselt number, and Sherwood number are presented. This study has significant applications in an intra-uterine fluid motion with tiny particles in a non-pregnant uterus, and this situation is very important in examining the embryo motion in the uterus.

2. Mathematical Formulation

We consider a peristaltic flow of MHD hyperbolic tangent nanofluid through a non-Darcy porous medium in a two-dimensional tapered asymmetric channel of width $\boldsymbol{2d}$ inclined at an angle $\boldsymbol{\alpha}$ as shown in figure 1. The flow is induced due to the sinusoidal waves traveling along the tapered asymmetric walls with constant speed $\boldsymbol{c}$. The Cartesian coordinates are assumed in which the $\boldsymbol{X}$-axis lies along the channel axis, while the $\boldsymbol{Y}$-axis is perpendicular to it. Also, the velocity components $\boldsymbol{U}$ and $\boldsymbol{V}$ lie along $\boldsymbol{X}$ and $\boldsymbol{Y}$ directions, respectively. The geometry of the lower wall $\boldsymbol{y = H_1}$ and the upper wall $\boldsymbol{y = H_2}$ of the channel can be describe as

$$\boldsymbol{y = H_1(X,t) = -d - m'X - b_1 \sin\left[\frac{2\pi}{\lambda}(X - ct) + \varphi\right]} \quad (1)$$

$$\boldsymbol{y = H_2(X,t) = d + m'X + b_2 \sin\left[\frac{2\pi}{\lambda}(X - ct)\right]} \quad (2)$$

where $\boldsymbol{m'}$ is the non-uniform parameter of the tapered asymmetric channel, $\boldsymbol{b_1}$ and $\boldsymbol{b_2}$ are the amplitudes of lower and upper walls, $\boldsymbol{\lambda}$ is the wavelength, and $\boldsymbol{\varphi}$ denotes the phase difference which varies in the range $\boldsymbol{0 \le \varphi \le \pi}$. Note that $\boldsymbol{\varphi = 0}$ corresponds to asymmetric channel with waves out of phase, i.e., the both walls are moving outward or inward simultaneously. Moreover, $\boldsymbol{b_1}$, $\boldsymbol{b_2}$, $\boldsymbol{d}$, and $\boldsymbol{\varphi}$ satisfy the following condition

$$\boldsymbol{b_1^2 + b_2^2 + 2b_1b_2\cos\varphi \le (2d)^2} \quad (3)$$

Here, we assume the fluid to be electrically conducting in the presence of a uniform magnetic field $\boldsymbol{B = (0, 0, B_0)}$ applied in the $\boldsymbol{z}$-direction. The current density $\boldsymbol{J}$ including the Hall effect can be expressed after ignoring the ion-slip effect as follows [22]

$$\boldsymbol{J = \sigma_f(E + V \times B) - \frac{\sigma}{en_e}(J \times B)} \quad (4)$$

where $\boldsymbol{\sigma_f}$ is the electric conductivity of the fluid $\boldsymbol{E}$ is the electric field, $\boldsymbol{V}$ is the vector velocity, $\boldsymbol{e}$ is the electric charge and $\boldsymbol{n_e}$ is the number density of electrons. The induced magnetic field and electric field are ignored for a small Reynolds magnetic number with no polarization voltage. Therefore, equation (4) can be rewritten as follows

$$\boldsymbol{J = \frac{\sigma_f B_0}{1+m^2}[\,(V + mU)\hat{i} + (mV - U)\hat{j}\,]} \quad (5)$$

where $\boldsymbol{m = \frac{\sigma B_0}{en_e}}$ is the Hall parameter. Lorentz force per unit volume $\boldsymbol{J \times B}$ and Joule heating $\boldsymbol{\frac{JJ}{\sigma_f}}$ can be obtained through equation (5) as follows

$$\boldsymbol{F = J \times B = \frac{\sigma_f B_0^2}{1+m^2}[\,(mV - U)\hat{i} - (V + mU)\hat{j}\,]} \quad (6)$$

$$\boldsymbol{\frac{JJ}{\sigma_f} = \frac{\sigma_f B_0^2}{1+m^2}(V^2 + U^2)} \quad (7)$$

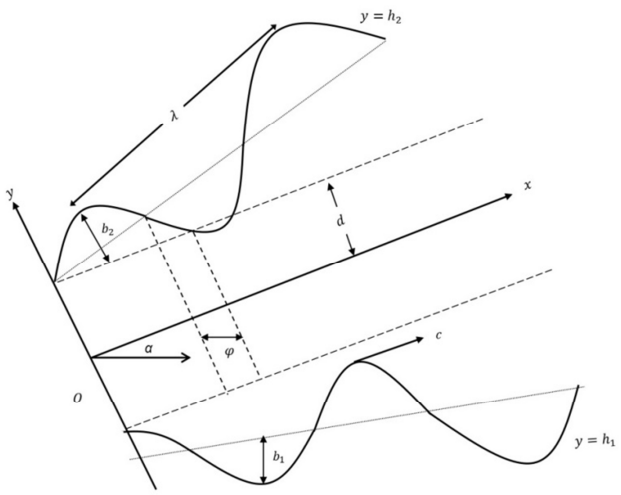

Figure 1: Geometry of the problem

The constitutive equation that obeys the behavior of hyperbolic tangent fluid is defined as [13, 14]

$$\boldsymbol{S = -[\eta_\infty + (\eta_0 + \eta_\infty)\tanh(\Gamma\dot{\gamma})^n]\dot{\gamma}} \quad (8)$$

where $\boldsymbol{S}$ is the extra stress tensor, $\boldsymbol{\eta_\infty}$ is the infinite shear rate viscosity, $\boldsymbol{\eta_0}$ is the zero shear rate

viscosity, $\boldsymbol{n}$ is the power law index, $\boldsymbol{\Gamma}$ is the time constant, and $\dot{\boldsymbol{\gamma}}$ is defined as follows

$$\dot{\boldsymbol{\gamma}} = \sqrt{\frac{1}{2}\sum_i \sum_j \dot{\boldsymbol{\gamma}}_{ij}\, \dot{\boldsymbol{\gamma}}_{ji}} = \sqrt{\frac{1}{2}\boldsymbol{\Pi}} \tag{9}$$

where $\boldsymbol{\Pi} = \boldsymbol{trac}(\boldsymbol{gradV} + (\boldsymbol{gradV})^{\boldsymbol{T}})$ is the second invariant strain tensor. Here, we consider equation (8) when $\boldsymbol{\eta_\infty} = \boldsymbol{0}$, and $\boldsymbol{\Gamma\dot{\gamma}} < \boldsymbol{1}$. Therefore, the component of extra stress tensor can be written as

$$\boldsymbol{S} = -\boldsymbol{\eta_0}(\boldsymbol{\Gamma\dot{\gamma}})^{\boldsymbol{n}}\dot{\boldsymbol{\gamma}} = -\boldsymbol{\eta_0}(\boldsymbol{1} + \boldsymbol{\Gamma\dot{\gamma}} - \boldsymbol{1})^{\boldsymbol{n}}\dot{\boldsymbol{\gamma}} = -\boldsymbol{\eta_0}\big(\boldsymbol{1} + \boldsymbol{n}(\boldsymbol{\Gamma\dot{\gamma}} - \boldsymbol{1})\big)\dot{\boldsymbol{\gamma}} \tag{10}$$

Eq. (10) in component form is defined as follows

$$\boldsymbol{S_{XX}} = -\boldsymbol{2\eta_0}[\boldsymbol{1} + \boldsymbol{n}(\boldsymbol{\Gamma\dot{\gamma}} - \boldsymbol{1})]\frac{\boldsymbol{\partial U}}{\boldsymbol{\partial X}} \tag{11}$$

$$\boldsymbol{S_{XY}} = \boldsymbol{S_{YX}} = -\boldsymbol{\eta_0}[\boldsymbol{1} + \boldsymbol{n}(\boldsymbol{\Gamma\dot{\gamma}} - \boldsymbol{1})]\left(\frac{\boldsymbol{\partial U}}{\boldsymbol{\partial Y}} + \frac{\boldsymbol{\partial V}}{\boldsymbol{\partial X}}\right) \tag{12}$$

$$\boldsymbol{S_{YY}} = -\boldsymbol{2\eta_0}[\boldsymbol{1} + \boldsymbol{n}(\boldsymbol{\Gamma\dot{\gamma}} - \boldsymbol{1})]\frac{\boldsymbol{\partial V}}{\boldsymbol{\partial Y}} \tag{13}$$

$$\dot{\boldsymbol{\gamma}} = \left(\boldsymbol{2}\left(\frac{\boldsymbol{\partial U}}{\boldsymbol{\partial X}}\right)^{\boldsymbol{2}} + \left(\frac{\boldsymbol{\partial U}}{\boldsymbol{\partial Y}} + \frac{\boldsymbol{\partial V}}{\boldsymbol{\partial X}}\right)^{\boldsymbol{2}} + \boldsymbol{2}\frac{\boldsymbol{\partial V}}{\boldsymbol{\partial Y}}\right)^{\boldsymbol{1/2}} \tag{14}$$

Hence, the equations governing the flow for the inclined channel of MHD hyperbolic tangent nanofluid through a non-Darcy porous medium in the presence of Brownian motion, thermophoresis, couple stresses, radiation, Joule heating, viscous dissipation, chemical reaction and activation energy, heat generation/absorption, and thermal diffusion and diffusion thermo effects may be written as [27-36]

$$\frac{\boldsymbol{\partial U}}{\boldsymbol{\partial X}} + \frac{\boldsymbol{\partial V}}{\boldsymbol{\partial Y}} = \boldsymbol{0} \tag{15}$$

$$\boldsymbol{\rho_f}\left(\frac{\boldsymbol{\partial U}}{\boldsymbol{\partial t}} + \boldsymbol{U}\frac{\boldsymbol{\partial U}}{\boldsymbol{\partial X}} + \boldsymbol{V}\frac{\boldsymbol{\partial U}}{\boldsymbol{\partial Y}}\right) = -\frac{\boldsymbol{\partial P}}{\boldsymbol{\partial X}} + \frac{\boldsymbol{\partial S_{XX}}}{\boldsymbol{\partial X}} + \frac{\boldsymbol{\partial S_{XY}}}{\boldsymbol{\partial Y}} - \boldsymbol{\rho_f g}\sin\boldsymbol{\alpha}\,\big(\boldsymbol{\beta_T}(\boldsymbol{T} - \boldsymbol{T_0}) + \boldsymbol{\beta_C}(\boldsymbol{C} - \boldsymbol{C_0})\big) - \frac{\boldsymbol{\sigma B_0^2}}{\boldsymbol{1+m^2}}(\boldsymbol{V} - \boldsymbol{mU}) - \boldsymbol{\eta_1}\frac{\boldsymbol{\partial^4 U}}{\boldsymbol{\partial Y^4}} - \frac{\boldsymbol{\mu_f}}{\boldsymbol{k_1}}\boldsymbol{U} - \frac{\boldsymbol{\rho_f}\,\boldsymbol{C_b}}{\sqrt{\boldsymbol{k_1}}}\boldsymbol{U^2} \tag{16}$$

$$\boldsymbol{\rho_f}\left(\frac{\boldsymbol{\partial V}}{\boldsymbol{\partial t}} + \boldsymbol{U}\frac{\boldsymbol{\partial V}}{\boldsymbol{\partial X}} + \boldsymbol{V}\frac{\boldsymbol{\partial V}}{\boldsymbol{\partial Y}}\right) = -\frac{\boldsymbol{\partial P}}{\boldsymbol{\partial Y}} + \frac{\boldsymbol{\partial S_{XY}}}{\boldsymbol{\partial X}} + \frac{\boldsymbol{\partial S_{YY}}}{\boldsymbol{\partial Y}} - \boldsymbol{\rho_f g}\cos\boldsymbol{\alpha}\,\big(\boldsymbol{\beta_T}(\boldsymbol{T} - \boldsymbol{T_0}) + \boldsymbol{\beta_C}(\boldsymbol{C} - \boldsymbol{C_0})\big) - \frac{\boldsymbol{\sigma B_0^2}}{\boldsymbol{1+m^2}}(\boldsymbol{V} + \boldsymbol{mU}) - \boldsymbol{\eta_1}\frac{\boldsymbol{\partial^4 V}}{\boldsymbol{\partial Y^4}} - \frac{\boldsymbol{\mu_f}}{\boldsymbol{k_1}}\boldsymbol{V} - \frac{\boldsymbol{\rho_f}\,\boldsymbol{C_b}}{\sqrt{\boldsymbol{k_1}}}\boldsymbol{V^2} \tag{17}$$

$$(\boldsymbol{\rho c})_f\left(\frac{\boldsymbol{\partial T}}{\boldsymbol{\partial t}} + \boldsymbol{U}\frac{\boldsymbol{\partial T}}{\boldsymbol{\partial X}} + \boldsymbol{V}\frac{\boldsymbol{\partial T}}{\boldsymbol{\partial Y}}\right) = \boldsymbol{\kappa_f}\left(\frac{\boldsymbol{\partial^2 T}}{\boldsymbol{\partial X^2}} + \frac{\boldsymbol{\partial^2 T}}{\boldsymbol{\partial Y^2}}\right) - \frac{\boldsymbol{\partial q_r}}{\boldsymbol{\partial Y}} + \left(\boldsymbol{S_{XX}}\frac{\boldsymbol{\partial U}}{\boldsymbol{\partial X}} + \boldsymbol{S_{XY}}\left(\frac{\boldsymbol{\partial U}}{\boldsymbol{\partial Y}} + \frac{\boldsymbol{\partial V}}{\boldsymbol{\partial X}}\right) + \boldsymbol{S_{YY}}\frac{\boldsymbol{\partial V}}{\boldsymbol{\partial Y}}\right) + (\boldsymbol{\rho c})_p\left[\boldsymbol{D_B}\left(\frac{\boldsymbol{\partial C}}{\boldsymbol{\partial X}}\frac{\boldsymbol{\partial T}}{\boldsymbol{\partial X}} + \frac{\boldsymbol{\partial C}}{\boldsymbol{\partial Y}}\frac{\boldsymbol{\partial T}}{\boldsymbol{\partial Y}}\right) + \frac{\boldsymbol{D_T}}{\boldsymbol{T_m}}\left(\left(\frac{\boldsymbol{\partial T}}{\boldsymbol{\partial X}}\right)^{\boldsymbol{2}} + \left(\frac{\boldsymbol{\partial T}}{\boldsymbol{\partial Y}}\right)^{\boldsymbol{2}}\right)\right] + \frac{\boldsymbol{D_B K_T}}{\boldsymbol{c_s}}\left(\frac{\boldsymbol{\partial^2 C}}{\boldsymbol{\partial X^2}} + \frac{\boldsymbol{\partial^2 C}}{\boldsymbol{\partial Y^2}}\right) + \frac{\boldsymbol{\sigma_f B_0^2}}{\boldsymbol{(1+m^2)}}\big(\boldsymbol{U^2} + \boldsymbol{V^2}\big) + \boldsymbol{\Phi_0}(\boldsymbol{T} - \boldsymbol{T_0}) \tag{18}$$

$$\frac{\boldsymbol{\partial C}}{\boldsymbol{\partial t}} + \boldsymbol{U}\frac{\boldsymbol{\partial C}}{\boldsymbol{\partial X}} + \boldsymbol{V}\frac{\boldsymbol{\partial C}}{\boldsymbol{\partial Y}} = \boldsymbol{D_B}\left(\frac{\boldsymbol{\partial^2 C}}{\boldsymbol{\partial X^2}} + \frac{\boldsymbol{\partial^2 C}}{\boldsymbol{\partial Y^2}}\right) + \left(\frac{\boldsymbol{D_T} + \boldsymbol{D_B}\,\boldsymbol{K_T}}{\boldsymbol{T_m}}\right)\left(\frac{\boldsymbol{\partial^2 T}}{\boldsymbol{\partial X^2}} + \frac{\boldsymbol{\partial^2 T}}{\boldsymbol{\partial Y^2}}\right) - \boldsymbol{K_r^2}\,(\boldsymbol{C} - \boldsymbol{C_0})\left(\frac{\boldsymbol{T}}{\boldsymbol{T_0}}\right)\boldsymbol{exp}\left(-\frac{\boldsymbol{E_a}}{\boldsymbol{k}\,\boldsymbol{T}}\right) \tag{19}$$

The corresponding boundary conditions are given as [5]

$$\boldsymbol{U} = \boldsymbol{0}, \frac{\boldsymbol{\partial^2 U}}{\boldsymbol{\partial^2 Y}} = \boldsymbol{0},\ \boldsymbol{T} = \boldsymbol{T_0}, \boldsymbol{C} = \boldsymbol{C_0}, \text{ at } \boldsymbol{y} = \boldsymbol{H_1}$$

$$\boldsymbol{U} = \boldsymbol{0}, \frac{\boldsymbol{\partial^2 U}}{\boldsymbol{\partial^2 Y}} = \boldsymbol{0}, \boldsymbol{T} = \boldsymbol{T_1}, \boldsymbol{C} = \boldsymbol{C_1}, \text{ at } \boldsymbol{y} = \boldsymbol{H_2} \tag{20}$$

The radiative heat flux $\boldsymbol{q_r}$ is given by [37-40]

$$\boldsymbol{q_r} = \frac{\boldsymbol{-4\sigma^*}}{\boldsymbol{3k_R}}\frac{\boldsymbol{\partial T^4}}{\boldsymbol{\partial R}} \tag{21}$$

where $\boldsymbol{\sigma^*}$ is the Stefan-Boltzmann constant and $\boldsymbol{k_R}$ is the mean absorption coefficient. Here, the difference in temperature within the flow is sufficiently small. Thus, by expanding the term $\boldsymbol{T^4}$ in Taylor series about temperature $\boldsymbol{T_0}$ we obtain

$$\boldsymbol{T^4} = \boldsymbol{T_0^4} + \boldsymbol{4}\,\boldsymbol{T_0^3}(\boldsymbol{T} - \boldsymbol{T_0}) + \boldsymbol{6}\,\boldsymbol{T_0^2}\,(\boldsymbol{T} - \boldsymbol{T_0})^2 + \cdots \tag{22}$$

By neglecting higher order terms in equation (22) beyond the first order in $(\boldsymbol{T} - \boldsymbol{T_0})$, we get

$$\boldsymbol{T^4} \cong \boldsymbol{4}\,\boldsymbol{T_0^3}\boldsymbol{T} - \boldsymbol{3}\boldsymbol{T_0^4} \tag{23}$$

By substituting equation (23) into equation (21), we obtain

$$q_r = -\frac{16\,\sigma^* T_0^3}{3k_R}\frac{\partial T}{\partial Y} \tag{24}$$

Transformation between laboratory and moving frames is given as

$$y = Y,\ x = X - ct,\ p(x,y) = P(X,Y,t), u = U - c, v = V(x,y,t),\ T(x,y) = T(X,Y,t),\ C(x,y) = C(X,Y,t) \tag{25}$$

where (u, v) are the components of velocity in wave frame (x, y). Defining the following non-dimensional quantities

$$u^* = \frac{u}{c},\ v^* = \frac{v}{c\delta},\ x^* = \frac{x}{\lambda},\ y^* = \frac{y}{d},\ t^* = \frac{ct}{\lambda}, P^* = \frac{d^2 P}{c\lambda\mu_f},\ H_1 = \frac{h_1}{d},\ H_2 = \frac{h_2}{d},\ k' = \frac{m'\lambda}{d},\ a = \frac{b_1}{d},\ b = \frac{b_2}{d},\ \theta = \frac{T-T_0}{T_1-T_0},\ \phi = \frac{C-C_0}{C_1-C_0},\ S_{ij}^* = \frac{d}{c\mu_f}S_{ij},\ \epsilon = \frac{a}{d},\ Re = \frac{\rho_f c d}{\mu_f},\ \delta = \frac{d}{\lambda},\ M = \sqrt{\frac{\sigma}{\mu_f}}B_0 d,\ Pr = \frac{\mu_f c_p}{k_f},\ Ec = \frac{c^2}{c_{p(T_1-T_0)}},\ Br = Ec\,Pr,\ Da = \frac{k_1}{d^2},\ R = \frac{4\sigma^* T_0^3}{k_f k_R},\ Nb = \frac{\tau_1 D_B}{\nu}(C_1 - C_0),\ Nt = \frac{\tau_1 D_T}{\nu T_m}(T_1 - T_0),\ Sc = \frac{\nu}{D_B}, C_f = \frac{\rho_f C_b d^2 c}{\mu_f\sqrt{k_1}},\ Du = \frac{D_B K_T (C_1-C_0)}{\mu_f c_s c_f (T_1-T_0)},\ Sr = \frac{D_B K_T (T_1-T_0)}{\nu T_m (C_1-C_0)},\ Gr = \frac{\rho_f g \beta_T d^2 (T_1-T_0)}{c\mu_f},\ Gc = \frac{\rho_f g \beta_C d^2 (C_1-C_0)}{c\,\mu_f},\ \rho_1 = \frac{T_1-T_0}{T_0},\ E = \frac{E_a}{K T_0},\ \xi = \frac{K_r^2 d^2}{D_B},\ Q = \frac{Q_0 d^2}{\mu_f c_p},\ \gamma_1 = \sqrt{\frac{\mu_f}{\eta_1}}d,\ We = \frac{\Gamma c}{d} \tag{26}$$

Here, we assume Reynolds number and the wave number $\delta = (d/\lambda)$ to be small $(Re \approx 0, \delta \approx 0)$. By applying the transformation between laboratory and moving frames in equation (25) and using the non-dimensional quantities in equation (26), the equations of continuity, momentum, temperature, and nanoparticles concentration (15)-(19) can be rewritten after applying the low Reynolds number and long-wavelength approximations as follows

$$\frac{\partial u}{\partial x} + \frac{\partial v}{\partial y} = 0 \tag{27}$$

$$\frac{\partial P}{\partial x} = \frac{\partial S_{xy}}{\partial y} - (Gr\,\theta + \mathrm{Gc}\,\phi)\sin\alpha - \left(\frac{M^2}{1+m^2} + \frac{1}{Da}\right)(u+1) - C_f\,(u+1)^2 - \frac{1}{\gamma_1^2}\frac{\partial^4 u}{\partial y^4} \tag{28}$$

$$\frac{\partial P}{\partial y} = 0 \tag{29}$$

$$\left(1 + \frac{4}{3}R\right)\frac{\partial^2\theta}{\partial y^2} + Br\,S_{xy}\frac{\partial u}{\partial y} + Nb\,Pr\frac{\partial\phi}{\partial y}\frac{\partial\theta}{\partial y} + Nt\,Pr\left(\frac{\partial\theta}{\partial y}\right)^2 + Du\,Pr\frac{\partial^2\phi}{\partial y^2} + \frac{M^2\,Br}{1+m^2}(u+1)^2 + Q\,Pr\,\theta = 0 \tag{30}$$

$$\frac{\partial^2\phi}{\partial y^2} + \left(\frac{Nt}{Nb} + Sc\,Sr\right)\frac{\partial^2\theta}{\partial y^2} - \xi\,\phi\,(\rho_1\theta + 1)exp\left(-\frac{E}{(\rho_1\theta+1)}\right) = 0 \tag{31}$$

where,

$$S_{xy} = [1 + n(We\,\dot\gamma - 1)]\frac{\partial u}{\partial y},\ S_{xx} = S_{yy} = 0,\ \text{and}\ \dot\gamma = \left[\left(\frac{\partial u}{\partial y}\right)^2\right]^{1/2} \tag{32}$$

The boundary conditions in equation (20) can be rewritten in the dimensionless form as follows

$$u = 0, \frac{\partial^2 u}{\partial^2 y} = 0, \theta = \phi = 0, \text{at}\ y = h_1 = -1 - k'x - a\,sin\left[\frac{2\pi}{\lambda}(x - t) + \varphi\right]$$

$$u = 0, \frac{\partial^2 u}{\partial^2 y} = 0, \theta = \phi = 1, \text{at}\ y = h_2 = 1 + k'x + b\,sin\left[\frac{2\pi}{\lambda}(x - t)\right] \tag{33}$$

3. Method of Solution: Homotopy perturbation Method (HPM)

Semi-analytical results are produced by using homotopy perturbation method (HPM). HPM recommends to write equations (28), (30), and (31) as follows [41-45]

$$(1-p)\big((L_1(u) - L_1(u_0))\big) + p\left(L_1(w) - \frac{\partial S_{xy}}{\partial y} + (Gr\,\theta + \mathrm{Gc}\,\phi)\sin\alpha + \left(\frac{M^2}{1+m^2} + \frac{1}{Da}\right)(u+1) + C_f\,(u+1)^2\right) = 0 \tag{34}$$

$$(1-p)\big(L_2(\theta)-L_2(\theta_0)\big)+p\Bigg(L_2(\theta)+\frac{1}{\left(1+\frac{4}{3}R\right)}\Big(Br\,S_{xy}\frac{\partial u}{\partial y}+Nb\,Pr\frac{\partial\phi}{\partial y}\frac{\partial\theta}{\partial y}+Nt\,Pr\left(\frac{\partial\theta}{\partial y}\right)^2+Du\,Pr\frac{\partial^2\phi}{\partial y^2}+\frac{M^2\,Br}{1+m^2}(u+1)^2+Q\,Pr\,\theta\Big)\Bigg)=0 \quad (35)$$

$$(1-p)\big(L_2(\phi)-L_2(\phi_0)\big)+p\Bigg(L_2(\phi)+\left(\frac{Nt}{Nb}+Sc\,Sr\right)L_2(\theta)-\xi\,\phi\,(\rho_1\theta+1)exp\left(-\frac{E}{(\rho_1\theta+1)}\right)\Bigg)=0 \quad (36)$$

with $L_1=\frac{1}{\gamma_1^2}\frac{\partial^4}{\partial y^4}+\frac{\partial P}{\partial x}$, and $l_2=\frac{\partial^2}{\partial y^2}$ as the linear operators. The initial boundary conditions u_0, θ_0, and ϕ_0 are given as

$$u_0=\frac{1}{24}(h_1-y)(h_2-y)\big(h_1^2+h_2^2+h_2\,y-y^2+h_1(-3h_2+y)\big)\gamma_1^2\frac{\partial P}{\partial x},\ \theta_0=\phi_0=\frac{h_1-y}{h_1-h_2} \quad (37)$$

The solution of u, θ, and ϕ can be expressed in terms of power series form as follows

$$(u,\theta,\phi)=(u_0,\theta_0,\phi_0)+p\,(u_1,\theta_1,\phi_1)+p^2\,(u_2,\theta_2,\phi_2)+\cdots \quad (38)$$

where $p\in[0,1]$ is the embedding parameter. The solution of velocity, temperature, and nanoparticle concentration for $p=1$ may be written as follows:

$$u(x,y)=\frac{1}{24}(h_1-y)(h_2-y)\big(h_1^2+h_2^2+h_2\,y-y^2+h_1(-3h_2+y)\big)\gamma_1^2\frac{\partial P}{\partial x}+c_1y+c_2y^2+c_3y^3+c_4y^4+c_5y^5+c_6y^6+c_7y^7+c_8y^8+c_9y^9+c_{10}y^{10}+c_{11}y^{11}+c_{12}y^{12}+c_{13}y^{13}+c_{14}y^{14}+c_{15}y^{15}+c_{16}y^{16}+c_{17}y^{17}++c_{18}y^{18}+c_{19}y^{19}+c_{20}y^{20}+c_{21} \quad (39)$$

$$\theta(x,y)=\frac{h_1-y}{h_1-h_2}+c_{22}y+c_{23}y^2+c_{24}y^3+c_{25}y^4+c_{26}y^5+c_{27}y^6+c_{28}y^7+c_{29}y^8+c_{30}y^9+c_{31}y^{10}+c_{32}y^{11}+c_{33}y^{12}+c_{34}y^{13}+c_{35}y^{14}+c_{36}y^{15}+c_{37}y^{16}+c_{38}y^{17}++c_{39}y^{18}+c_{40}y^{19}+c_{41} \quad (40)$$

$$\phi(x,y)=\frac{h_1-y}{h_1-h_2}+c_{42}y+c_{43}y^2+c_{44}y^3+c_{45}y^4+c_{46}y^5+c_{47}y^6+c_{48}y^7+c_{49}y^8+c_{50}y^9+c_{51}y^{10}+c_{52}y^{11}+c_{53}y^{12}+c_{54}y^{13}+c_{55}y^{14}+c_{56} \quad (41)$$

Here, c_1 - c_{56} are not given here to save space, but they are available upon request. Heat transfer coefficient $Z(x)$, Nusselt number Nu, and Sherwood number Sh at the upper wall of the channel are defined as follows [26]

$$Z(x)=\frac{\partial h_2}{\partial x}\left(\frac{\partial\theta}{\partial y}\right)_{y\to h_2},\ Nu=-\left(\frac{\partial\theta}{\partial y}\right)_{y\to h_2},\ Sh=-\left(\frac{\partial\phi}{\partial y}\right)_{y\to h_2} \quad (42)$$

we obtained the above expressions by substituting equations (39)-(41) into equation (42), and then we used the software Mathematica package to evaluate them numerically for different parameters of the problem.

4. Entropy generation

The entropy generation equation is modified by involving Joule heating, radiation, and heat generation/absorption as follows [18]

$$Ns=\left(\frac{\partial\theta}{\partial y}\right)^2+\frac{1}{\left(1+\frac{4}{3}R\right)}\Big(Br\,S_{xy}\frac{\partial u}{\partial y}+Nb\,Pr\frac{\partial\phi}{\partial y}\frac{\partial\theta}{\partial y}+Nt\,Pr\left(\frac{\partial\theta}{\partial y}\right)^2+Du\,Pr\frac{\partial^2\phi}{\partial y^2}+\frac{M^2\,Br}{1+m^2}(u+1)^2+Q\,Pr\,\theta\Big) \quad (43)$$

5. Results and discussion

In this section, we present a set of figures to analyse the behaviour of some parameters of MHD peristaltic flow of hyperbolic tangent nanofluid through a non-Darcy porous medium in an inclined tapered asymmetric channel. Here, we obtained the velocity, temperature and nanoparticle concentration profiles by taking the following fixed values $R=t=k'=\rho_1=We=Da=0.1$, $Du=x=a=0.2$, $b=0.3$, $Sr=C_f=\xi=\gamma_1=0.5$, $Sc=0.8$, $Nt=Nb=Pr=Br=Q=m=n=1$, $M=Gr=Gc=E=2$, $\alpha=\frac{\pi}{6}$, $\varphi=\frac{\pi}{2}$, $\frac{dP}{dx}=10$. Furthermore, we obtained plots of the impact of various parameters on heat transfer coefficient, Nusselt number, Sherwood number and entropy generation.

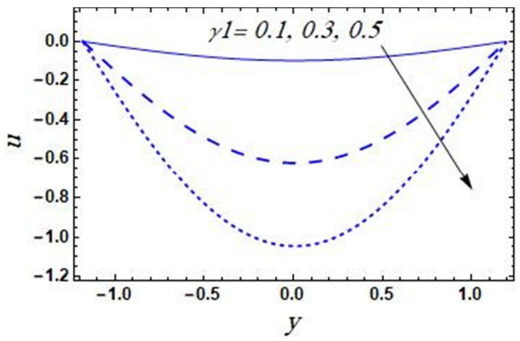

Figure 2: Variation of $\gamma_1$on u

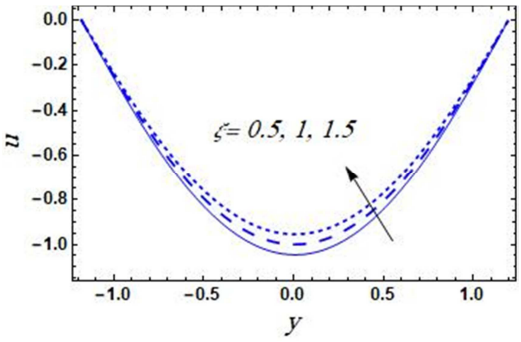

Figure 3: Variation of ξ on u

The variation of the velocity distribution u along the normal axis y for different values of of the couple stress parameter $\gamma_1$and the chemical reaction parameter ξ is illustrated in figures (2) and (3), respectively. We observed from these figures that the velocity u decreases rapidly with an increase of γ_1, while it increases by increasing ξ. The results in figure (2) may be due to the fact that the couple stresses spending some energy to rotate the fluid nanoparticles, and by that reducing the velocity. However, once the chemical reaction starts the friction and collisions between the fluid naoprticles increase, thus, the velocity enhances.

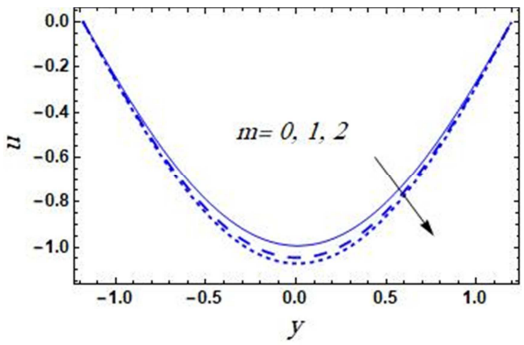

Figure 4: Variation of m on u

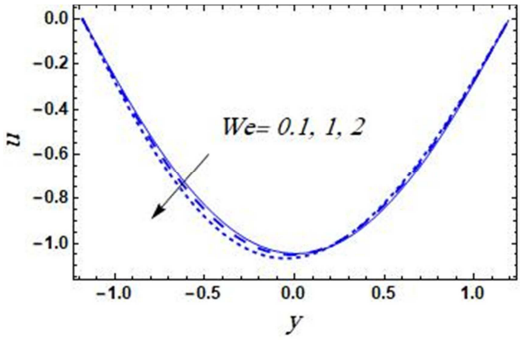

Figure 5: Variation of We on u

Moreover, we noticed from these figures that the velocity profile is parabolic. We also observed from that the velocity u for various values of γ_1 and ξ becomes lower along the normal axis y to reach the minimum value at the centre of the channel (at $y = 0$), after which it increases again. Note that the minimum value of the velocity u decreases with an increase of γ_1, while it increases as ξ increases. Further, figures (4) shows that the effect of Hall parameter m on the velocity profile u is similar to the effect of γ_1 that is given in figure (2). but the curves that describe the effect of m on velocity profile u are closer to each other comparing to those curves in figure (2). Physically, an increase in Hall parameter m causes a reduction in the electrical conductivity which reduces the damping force of magnetic strength, and accordingly, the velocity is increased. The influence of Br, Nt, Nb, Q, Da, a, b and k' is found to be similar to the effect of m that is captured in figure (3). Also, the impact of Gr and Gc on the

velocity profile u is extremely close to the effect of γ_1 that is given in figure (2). Moreover, the effect of R, n, C_f, M, E, ρ_1, and α on the velocity u is comparable to the impact of ξ that is displayed in figure (3). Note that these figures are omitted here for want of space. Fig. (5) shows the behavior of the velocity distribution with the normal axis y for various values of the Weissenberg number We. We observed that the velocity u has a dual behavior under the infuence of We. Fig. (5) shows that the behaviour of the velocity u changes at $y = 0.2$, in which it decreases by increasing the value of We in the interval $-1.2 \leq y \leq 0.2$, while it increases with an increases of We in the interval $0.2 \leq y \leq 1.2$. Further, figure (5) depicts that velocity profile u becomes lower along the normal axis y till reaches the maximum value at the central part of the channel, after which it increases.

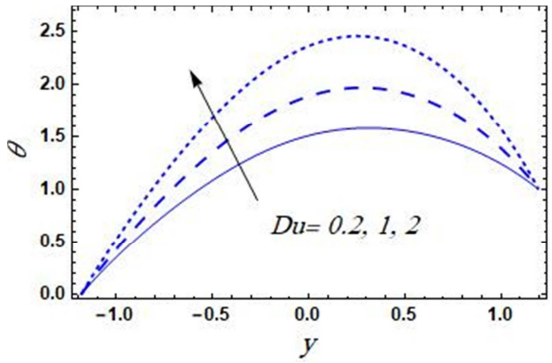

Figure 6: Variation of Du on θ

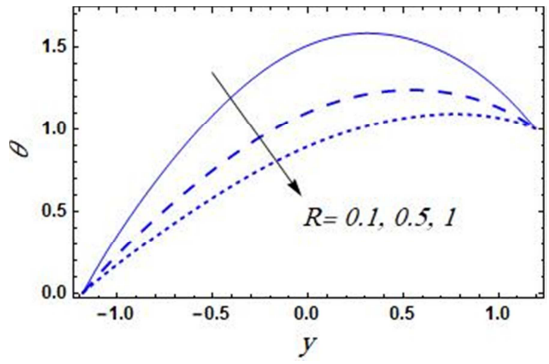

Figure 7: Variation of R on θ

Figs. (6) and (7) show the behavior of the temperature distribution θ with the normal axis y for various values of the Dufour number Du and radiation parameter R, respectively. We observed that the temperature increases as Du increases, while it decreases by increasing R. Actually, Dufour number Du is involved in temperature equation by concentration gradient. Therefore, an increase in the value of Du enhances the concentration gradient which accordingly rises the temperature. Physically, an increase in Dufour number Du results in a decrease in the fluid viscosity, thus, the velocity enhances which accordingly increases the temperature due to the movement of the fluid particles with faster molecular vibrations. Further, radiation reduces the energy which causes a decay in the temperature. It is clear from figures (6) and (7) that the change of the temperature θ along the normal axis y becomes greater and reaches the maximum value, after which it decreases. Note that the maximum value of θ increases by increasing the value of Du, whereas it decreases with an increase of R. We found that the effect of γ_1, n, m, C_f, Gr and Gc on temperature θ is similar to the effect of R that is capted in figure (7). But, the cuves that are obtained for , m, C_f, Gr and Gc are closer to each other comparing with those that obtained for R. Note that thses plots are not provided here to aviod any kind of duplication. Figs. (8) and (9) illustrate the influence of Weissenberg number We, and thermophoresis parameter Nt on the temperature profile θ against the normal axis y. It is clear that the temperature has a dual behavior under the effect of the both We and Nt.

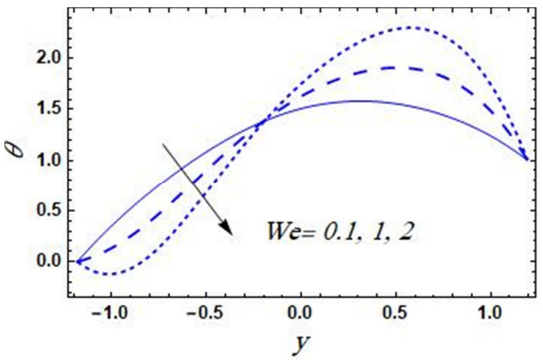

Figure 8: Variation of We on θ

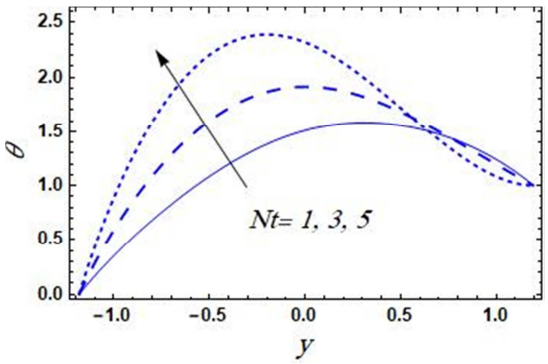

Figure 9: Variation of Nt on θ

Fig. (8) shows that the temperature decreases with the increase of We in the interval $-1.2 \leq y \leq -0.2$, while it increases by increasing We in the interval $-0.2 \leq y \leq 1.2$. Fig. (9) illustrates that as Nt increases, the temperature increases in the interval $-1.2 \leq y \leq 0.6$, whereas it decreases by increasing Nt in the interval $0.6 \leq y \leq 1.2$. Figs. (8) and (9) show that the curves of the influence of We on the temperature intersect at $y = -0.2$, while the curves o Nt intersect at $y = 0.6$. Moreover, the change of the temperature θ for different values of We and Nt along the normal axis y becomes greater and reaches the maximum value, after which it decreases. Note that the maximum value of θ increases by increasing the value of both We and Nt. The influence of Nb on temperature θ is found to be similar to the effect of Nt that is given in figure (9), and this figure is not given here to prevent any kind of duplication.

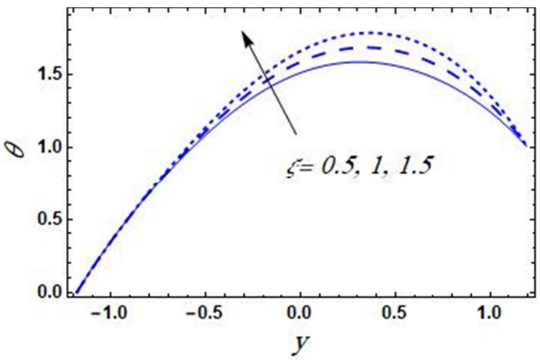

Figure 10: Variation of We on θ

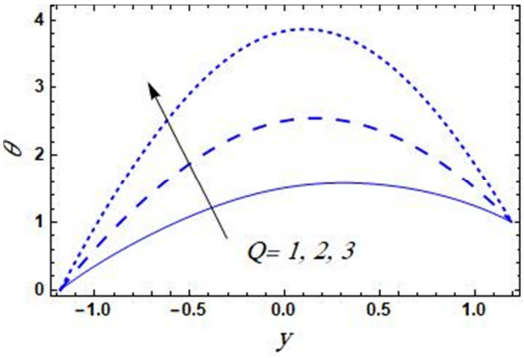

Figure 11: Variation of Q on θ

Fig. (10) shows that the effect of chemical reaction parameter ξ is comparable to the effect of Dufour number Du on the temperature profile that is given in figure (6). But, the chemical reaction parameter ξ does not affect the temperature profile in the interval $-1.2 \leq y \leq -0.3$. We also obtained similar effect on the temperature profile as in figure (10) for the activation energy parameter E and the temperature difference parameter ρ_1. Note that these figures are not displayed here for want of space. We observed from figure (11) that the influence of the heat generation/absorption parameter Q on the temperature profile is extremely close to the effect of Dufour number Du that is captured in figure (6). In fact, heat generation enhances the energy which enhances the temperature. Furthermore, the impact of different values of Br, M, Da, a, b, k' and α is similar to the effect of Du that is illustrated in figure

(6). But, the curves that obtained for Da and α are closer to each other comparing with the curves that obtained for Du. Note that these figures are not provided here to avoid any kind of repetition.

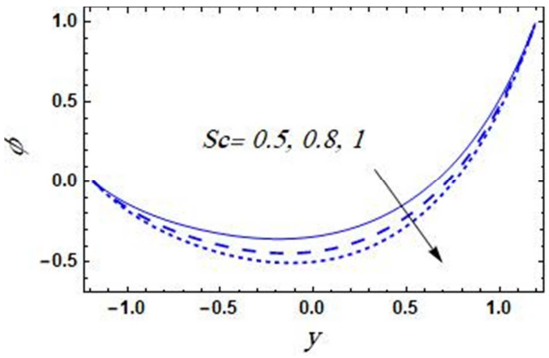

Figure 12: Variation of Sr on ϕ

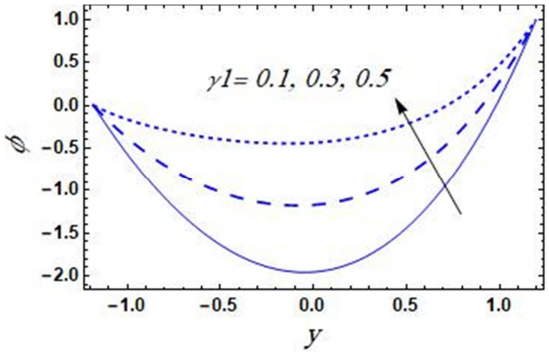

Figure 13: Variation of γ_1 on ϕ

The influence of Schmidt number Sc and the couple stress parameter γ_1 on the nanoparticle concentration distribution ϕ is depicted in figures (12) and (13), respectively. These graphs depict that the nanoparticle concentration ϕ decreases by increasing the value of Sc, whereas it increases with the increase of γ_1. Physically, an increase in the value of Sc reduces the mass diffusion rate, which causes the nanoparticles to move away with more speed. Thus, the nanoparticle concentration reduces. Additionally, the variation of the nanoparticle concentration distribution ϕ for various values of Sc and γ_1 becomes lower along the normal axis y to reach the lowest value at the central part of the channel, after which it increases and ends up with the maximum value. Note that the lowest value of ϕ decreases by increasing Sc, while it increases as γ_1 increases.

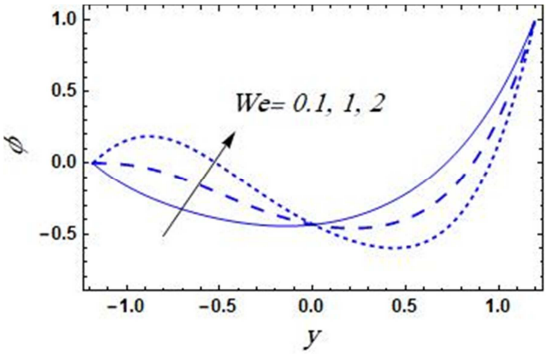

Figure 14: Variation of We on ϕ

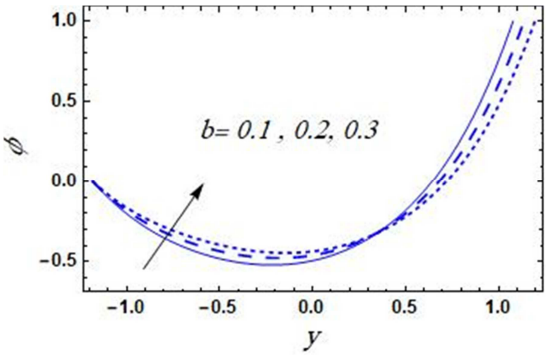

Figure 15: Variation of b on ϕ

Figs. (14) and (15) show that the nanoparticle concentration distribution ϕ has a dual behaviour under the influence of Weissenberg number We and amplitude of the upper wall b. Fig. (14) illustrates that the nanoparticle concentration profile ϕ increases with an increases of We in the interval $-1.2 \leq y \leq 0$, while it decreases by increasing We in the interval $0 \leq y \leq 1.2$. Fig. (14) shows that the curves intersect at $y = 0$. Further, the nanoparticle concentration distribution ϕ increases by increasing the value of amplitude of the upper wall b in the interval $-1.2 \leq y \leq 0.3$, whereas it decreases as b

increases in the interval $0.3 \leq y \leq 1.2$. Note that the curves in figure (15) intersect at $y = 0.3$.

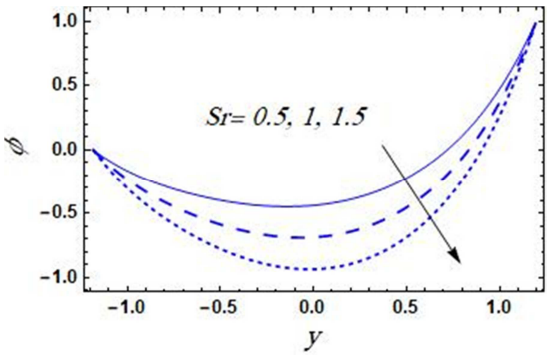

Figure 16: Variation of Sr on ϕ

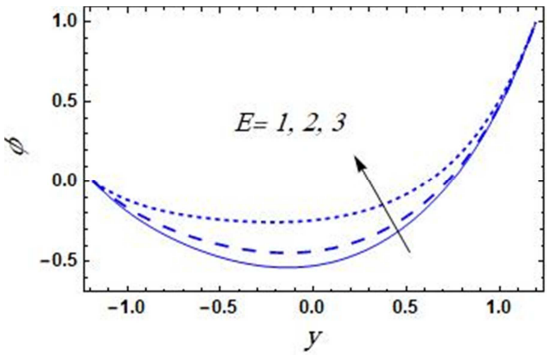

Figure 17: Variation of E on ϕ

Fig. (16) shows that the influence of Soret number Sr on that the nanoparticle concentration distribution ϕ is very close to the influence of Schmidt number Sc that is depicted in figure (12). Moreover, figure (17) illustrates that the influence of the activation energy parameter E is comparable of the influence of the couple stress parameter γ_1 on the nanoparticle concentration distribution ϕ that is shown in figure (13). Similar effect on nanoparticle concentration distribution ϕ to that given in figure (15) is obtained for k'. We also observed that the influence of Nt, Q, M and Br is comparable to the effect of Sc that is given in figure (12). Furthermore, the impact of R, E, Nb, n, m, ρ_1, and ξ on the nanoparticle concentration distribution ϕ is similar to that is given in figure (13). Note that these figures are not given here for want of space.

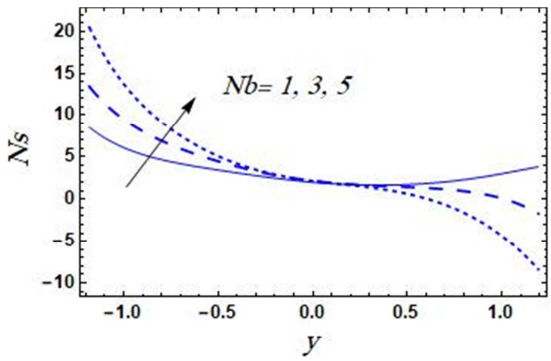

Figure 18: Variation of Nb on Ns

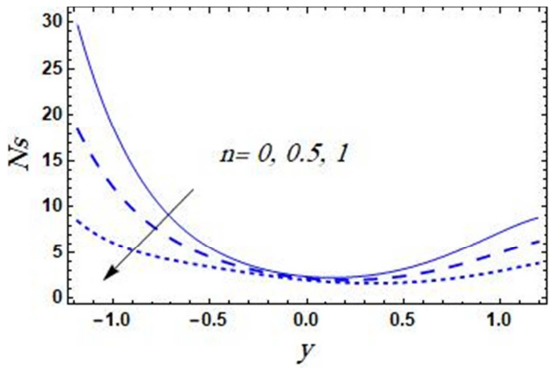

Figure 19: Variation of n on Ns

Fig. (18) and Fig. (19) are obtained to investigate the sequences of the Brownian motion parameter Nb and the power law index of hyperbolic tangent fluid model n on the entropy generation number Ns, respectively. These figures illustrate that the distribution of entropy generation number Ns has a dual behaviour under the effect of Nb and n. Fig. (18) depicts that the entropy generation number Ns increases by increasing the value of Nb in the interval $-1.2 \leq y \leq 0$, while it decrease as Nb increases in the interval $0 \leq y \leq 1.2$. However, it has an opposite behaviour under the effect of the hyperbolic tangent fluid model n. Note that the entropy generation number Ns decreases along the normal axis y with an increases in Nb. But, it increases along the normal axis y with the increase of n to reach the minimum value, after which it increases.

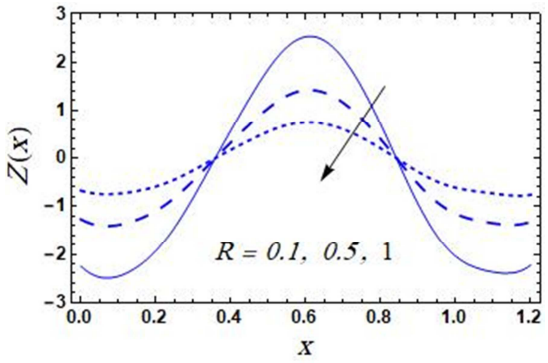

Figure 20: Variation of R on $Z(x)$

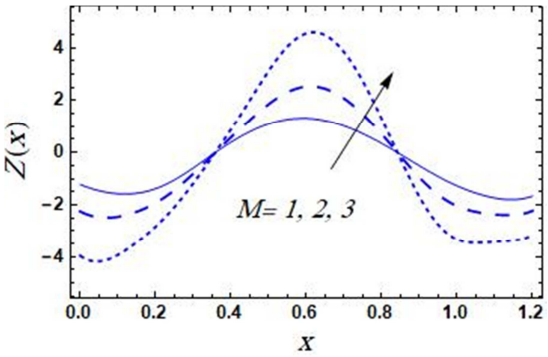

Figure 21: Variation of M on $Z(x)$

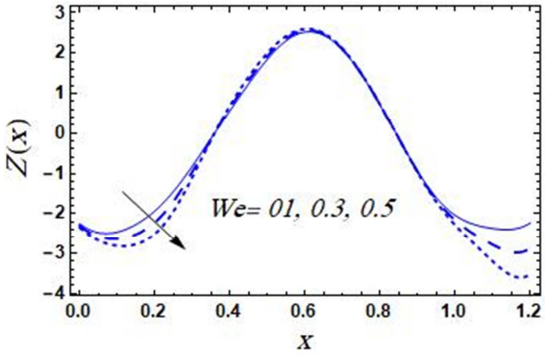

Figure 22: Variation of We on $Z(x)$

The variation in heat transfer coefficient $Z(x)$ with the parallel coordinate x for various values of the radiation parameter R and Hartman number M at the upper wall of the channel is displayed in figures (20) and (21), respectively. The dimensionless expression for heat transfer coefficient $Z(x)$ defines the rate of heat transfer or heat flux at the upper wall. It is clear from these figures that an oscillatory behavior occurs between $Z(x)$ and x-axis due to the propagation of the peristaltic waves along the channel walls. Fig. (20) shows that the absolute value of $Z(x)$ decreases with an increase in radiation parameter R. However, figure (21) depicts that the effect of Hartman number M on $Z(x)$ behaves in an opposite manner to the effect of R on $Z(x)$. We observed that the absolute value of $Z(x)$ increases slightly under the influence of We as displayed in figure (22).

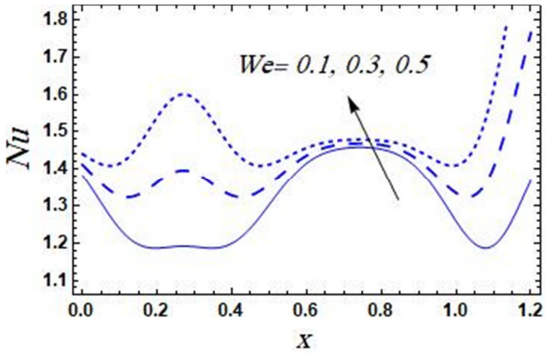

Figure 23: Variation of We on Nu

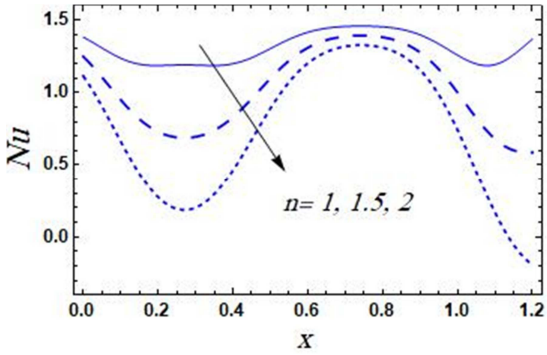

Figure 24: Variation of n on Nu

Figs. (23) and (24) depict the impact of Weissenberg number We and the power law index of hyperbolic tangent fluid model n on Nusselt number Nu. We observe from these graphs that an increase of We increases Nusselt number Nu, whereas Nu decreases with a increases in the power law index of hyperbolic tangent fluid model n. Furthermore, the relation between Nu and x-axis seems to be a wavy relation , i.e., Nu increases or decreases by increasing x-axis. It is clear from figure (23) that the minimum

value of Nu appears three times in one period, while Nu has a maximum value at the end of the period.

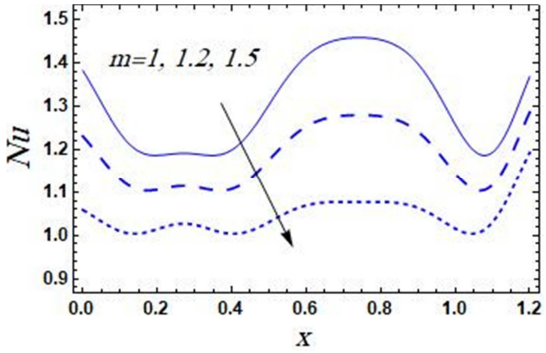

Figure 25: Variation of m on Nu

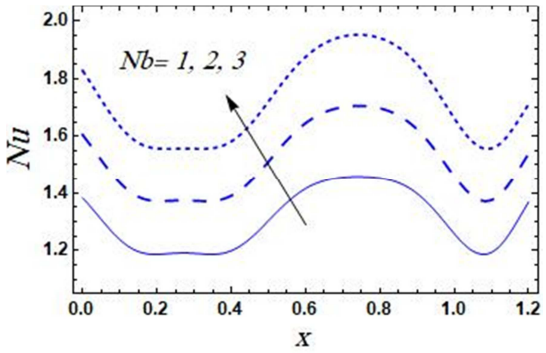

Figure 26: Variation of Nb on Nu

Fig. (24) shows that the maximum value of Nu appears three times in the same period, and Nu has a minimum value at the end of the period. Note that the curves of Nu for various values of We becomes more close to each other in the interval $0.6 \leq x \leq 0.9$. Moreover, the influence of Hall parameter m and the Brownian motion parameter Nb on Nusselt number Nu is illustrated in figures (25) and (26). We see from these figures that an increase of m dereases Nusselt number Nu, whereas Nu increases with an increases in Nb. Also, these figures show that the relation between Nu and x-axis seems to be a wavy relation , i.e., Nu increases or decreases by increasing x-axis. Figs. (25) and (26) show that Nu has a maximum value at $x = 0.7$, while the minimum value appears in three positions in one period.

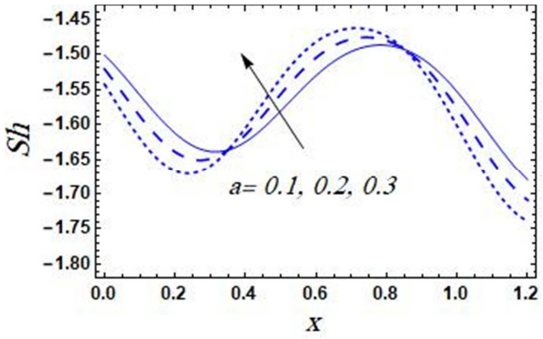

Figure 27: Variation of a on Sh

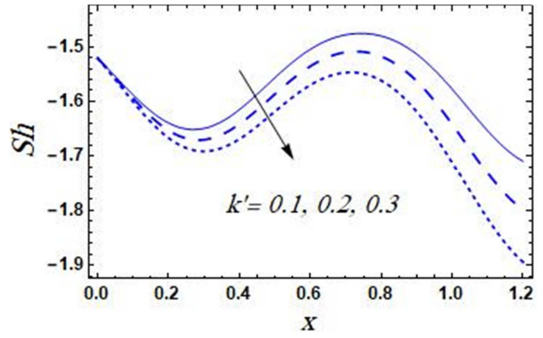

Figure 28: Variation of k' on Sh

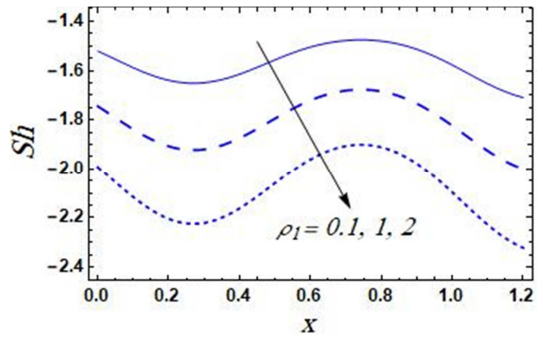

Figure 29: Variation of ρ_1 on Sh

The behavior of Sherwood number Sh with various values of the amplitude of the lower wall a and the non-uniform parameter of the tapered asymmetric channel k' is given in figures (27) and (28). The relation between Sh and x-axis seems to be a wavy relation, i.e., Sh increases or decreases by increasing x-axis. It is obvious from figure (27) that Sherwood number Sh has a dual behaviour under the influence of the amplitude of the lower wall a in

which it decreases in the interval $0.0 \leq x \leq 0.3 \cup 0.9 \leq x \leq 1.2$, while it increases in the interval $0.3 \leq x \leq 0.9$. Note that the curves for the influence of the amplitude of the lower wall a intersect at $x = 0.3$ and $x = 0.9$. Moreover, figure (28) shows that Sherwood number Sh decreases with an increase in the non-uniform parameter of the tapered asymmetric channel k'. Note that the curves that captured in figure (28) intersect at $x = 0$. Furthermore, the difference of the Sherwood number Sh for different values of a and k' becomes lower along parallel coordinate x, then it increases at $x = 0.3$, then it decreases again to end up with the minimum value. Note that the minimum value of Sherwood number Sh decreases by increasing the value of a and k'. Fig. (29) shows that the influence of the temperature difference parameter ρ_1 on Sherwood number Sh is comparable to the impact of k' that is given in figure (28), but the curves for ρ_1 do not intersect at any point.

6. Trapping phenomenon

Trapping is an interesting phenomenon in peristaltic transport that is referred to closed circulating streamlines that occur at high flow rates and for a very large occlusions. Streamlines under specified conditions in the wave frame split to trap a bolus moving with the wave speed. For incompressible fluids in two dimensional flow, we may consider a stream function $\psi(x, y)$ as follows

$$u = -\frac{\partial \psi}{\partial y}$$

Figs. (30) and (31) depict the influence of Forchheimer number C_f and the couple stress parameter $\gamma_1$on the trapping. These figures reveal that the trapped bolus decreases in size with an increase of Forchheimer number C_f, while it increases as γ_1 increases.

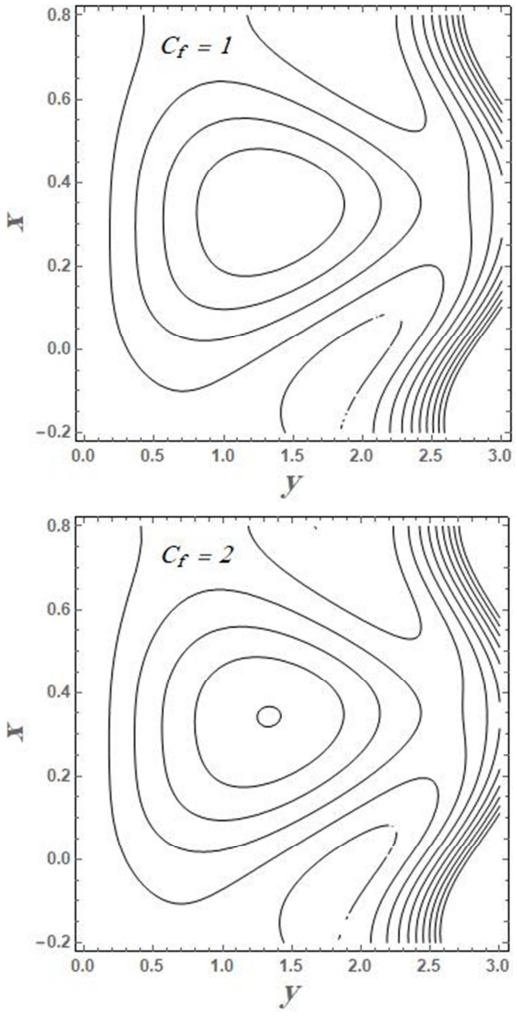

Figure 30: The streamlines contour is plotted for various values of C_f

7. Conclusion

In this study we discussed the influence of activation energyand cheical reaction, couple stresses, radiation, and Hall currents of peristaltic flow of MHD hyperbolic tangent nanofluid through a

non-Darcy porous medium in an inclined tapered asymmetric channel with heat and mass transfer.

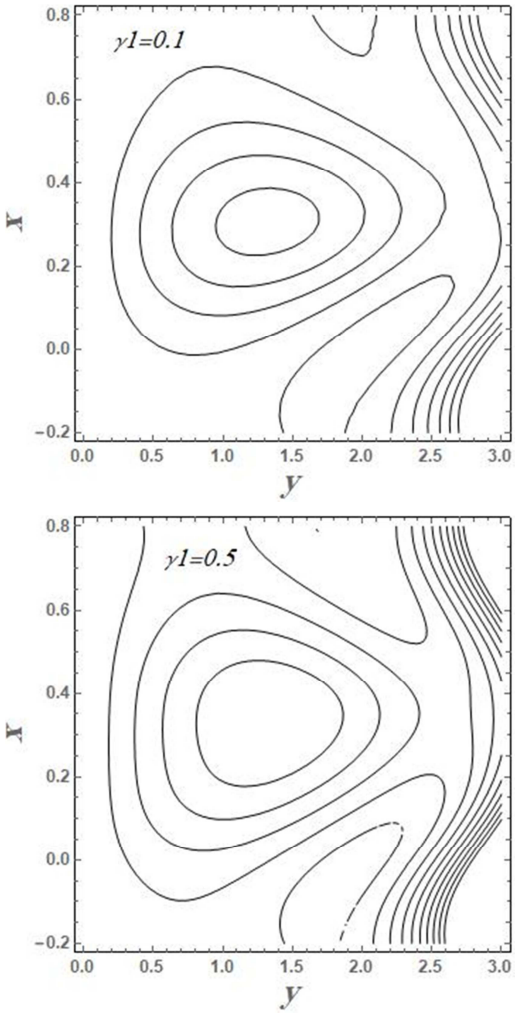

Figure 31: The streamlines contour is plotted for various values of γ_1

The impact of viscous dissipation, Joule heating, heat generation/absorption, and thermal diffusion and diffusion thermo effect is involved. The coupled non-linear equations governing the flow are simplified by using the long wavelength and low Reynolds number approximations. Then, the simplified equations are solved numerically by using a semi-analytical technique called homotopy perturbation method (HPM). Graphical results for velocity, temperature, and nanoparticle concentration profiles are obtained for various values of the involved parameters. Physical explanations of the obtained results have been provided [46-55]. Furthermore, graphs for heat transfer coefficient, entropy generation, Nusselt number, and Sherwood number have been presented. The key findings can be summed up as follows

1. Weissenberg number We has a dual behaviour on the velocity, temperature, and nanoparticle concentration profiles.

2. Thermophoresis parameter Nt and Brownian motion parameter Nb have a dual behavior on the temperature distribution, while they decreases the velocity.

3. Thermophoresis parameter Nt and Brownian motion parameter Nb affect the nanoparticle concentration profile in an opposite manner.

4. The velocity distribution decreases with an increases of γ_1, m, Br, Nt, Nb, Q, Da, a, b, Gr, Gc and k', while it increases by increasing the value of ξ, R, n, C_f, M, E, ρ_1, and α

5. The temperature profile enhances with an increase in Du, Q, Br, M, Da, a, b, k', α, ξ, ρ_1 and E, while it decreases with an increase in the value of R, γ_1, n, m, C_f, Gr and Gc.

6. The nanoparticle concentration profile decreases with an increases in Sc, Sr, Nt, Q, M and Br, while it increases by increasing each of γ_1, E, R, E, Nb, n, m, ρ_1, and ξ.

Nomenclature

U, V	velocity components in laboratory frame
u, v	velocity components in wave frame
X, Y	Cartesian coordinates in laboratory frame
r, z	Cartesian coordinates in wave frame
t	time
P	pressure

a amplitude of the lower wall
b amplitude of the upper wall
m', k' non-uniform parameter of the tapered asymmetric channel
φ phase difference
g acceleration due to gravity
Re Reynolds number
B_0 uniform magnetic field
T temperature
C concentration
D_T thermophoretic diffusion coefficient
K_T thermal diffusion ration
T_m fluid mean temperature
k_1 Permeability of the porous medium
D_B Brownian diffusion coefficient
c_s concentration susceptibility
Du Dufour number
Sc Schmidt number
Sr Soret number
η_1 couple stress constant
T_0 temperature at $y = h_1$
T_1 temperature at $y = h_2$
C_0 concentration at $y = h_1$
C_1 concentration at $y = h_2$
Ec Eckert number
Pr Prandtl number
Br Brinkman number
Φ_0 heat generation/absorption parameter
Q dimensional heat generation/absorption parameter
Nt thermophoresis parameter
Nb Brownian motion parameter
M Hartman number
η_∞ infinite shear rate viscosity for hyperbolic tangent fluid model
η_0 zero shear rate viscosity for hyperbolic tangent fluid model
n power law index for hyperbolic tangent fluid model
Γ time constant for hyperbolic tangent fluid model
We Weissenberg number
R radiation parameter
Da Darcy number
C_f Forchheimer number
Gr temperature Grashof number
Gc concentration Grashof number
β_T thermal expansion coefficient
β_C mass expansion coefficient
K_r^2 chemical reaction rate constant
$\frac{E_a}{k}$ activation energy over Boltzmann constant
γ_1 couple stress parameter
ξ chemical reaction parameter
E activation energy parameter
ρ_1 the temperature difference parameter
S_{xx}, S_{xy}, S_{yy} Extra stress tensor components

Greek symbols

ρ density
μ dynamic viscosity
σ electric conductivity
κ thermal conductivity
ν kinematic viscosity
δ wave number
θ dimensionless temperature
ϕ dimensionless nanoparticle concentration

Subscripts

f fluid
p nanoparticle

References

1. N.T. Eldabe, M. Gaber, and M.Y. Abou-zeid, Wall properties effect on the peristaltic motion of a coupled stress fluid with heat and mass transfer through a porous media. Journal of Engineering Mechanics, **142 (3)**, 04015102, (2015).
2. N.T. Eldabe, M.Y. Abou-zeid, and H. A. Ali, Effects of heat and mass transfer on Casson fluid between two co-axial tubes with peristalsis. Journal of advanced research in fluid mechanics and thermal science, **76**, 54–75, (2020).
3. N.T. El-Dabe, and M.Y. Abou-zeid, Radially varying magnetic field effect on peristaltic motion with heat and mass transfer of a non-Newtonian fluid between two co-axial tubes. Thermal Science, **22** (6A), 2449-2458, (2018).
4. N.T.M. Eldabe, M.Y. Abou-zeid, A. Abosaliem, A. Alana, and N. Hegazy, Homotopy perturbation approach for Ohmic dissipation and mixed convection effects on non-Newtonian nanofluid flow between two co-axial tubes with peristalsis. International Journal of Applied Electromagnetics and Mechanics, **67**, 153-163, (2021).
5. N.T. Eldabe, S. Elshabouri, H. Elarabawy, M.Y. Abouzeid, and A.J. Abuiyada, Wall properties and Joule heating effects on MHD peristaltic transport of Bingham non-Newtonian nanofluid. International Journal of Applied Electromagnetics and Mechanics, **69**, 87 – 106, (2022).
6. N.T. Eldabe, M.Y. Abou-zeid, M.A. Mohamed, and M. Maged, Peristaltic flow of Herschel

Bulkley nanofluid through a non-Darcy porous medium with heat transfer under slip condition. International Journal of Applied Electromagnetics and Mechanics, **66**, 649-668, (2021).

7. N. T. Eldabe, M.Y. Abou-zeid, M. E. Ouaf, D. R. Mustafa, and Y. M. Mohammed, Cattaneo – Christov heat flux effect on MHD peristaltic transport of Bingham nanofluid through a non – Darcy porous medium. International Journal of Applied Electromagnetics and Mechanics, **68**, 59-84, (2022).
8. N.T. Eldabe, G.M. Moatimid, M.Y. Abouzeid, A.A. ElShekhipy, and N.F. Abdallah, A semianalytical technique for MHD peristalsis of pseudoplastic nanofluid with temperature-dependent viscosity: Application in drug delivery system. Heat Transfer Research, **49**, 424–440, (2020).
9. N.T. Eldabe, G.M. Moatimid, M.Y. Abou-zeid, A.A. Elshekhipy, and N.F. Abdallah, Semi-analytical treatment of Hall current effect on peristaltic flow of Jeffery nanofluid. International Journal of Applied Electromagnetics and Mechanics, **7**, 47-66, (2021).
10. M.E. Ouaf, M.Y. Abouzeid, and Y.M. Younis, Entropy generation and chemical reaction effects on MHD non-Newtonian nanofluid flow in a sinusoidal channel, International Journal of Applied Electromagnetics and Mechanics, **69,** 45-65, (2022).
11. M.Y. Abou-zeid, Effects of thermal-diffusion and viscous dissipation on peristaltic flow of micropolar non-Newtonian nanofluid: Application of homotopy perturbation method. Results in Physics, **6**, 481–495 (2016).
12. N.T. Eldabe, M.Y. Abou-zeid, S.M. Elshabouri, T.N. Salama, and A.M. Ismael, Ohmic and viscous dissipation effects on micropolar non-Newtonian nanofluid Al2O3 flow through a non-Darcy porous media. International Journal of Applied Electromagnetics and Mechanics, **68**, 209–221 (2022).
13. R.Ellahi, A. Zeeshan, F. Hussain, and A. Asadollahi, Peristaltic Blood Flow of Couple Stress Fluid Suspended with Nanoparticles under the Influence of Chemical Reaction and Activation Energy. Symmetry, **11**, 276, (2019).
14. T. Hayat, A.A. Khanb , F. Bibib , and S. Farooqa, Activation energy and non-Darcy resistance in magneto peristalsis of Jeffrey material. Journal of Physics and Chemistry of Solids, **129**, 155-161, (2019).
15. Z. Nisar, T. Hayata, A. Alsaedi, and B. Ahmad, Significance of activation energy in radiative peristaltic transport of Eyring-powell nanofluid. International Communications in Heat and Mass Transfer, **116**, 104655, (2020).
16. T. Hayat, F. Bibi, S. Farooq, and A. A. Khan, Nonlinear radiative peristaltic flow of Jeffrey nanofluid with activation energy and modified Darcy's law. Journal of the Brazilian Society of Mechanical Sciences and Engineering, **41**, 296, (2019).
17. M. Ibrahim, N. Abdallah, and M. Abouzeid, Activation energy and chemical reaction effects on MHD Bingham nanofluid flow through a non-Darcy porous media. Egypt Journal of Chemistry, **65**, 137-144, (2022).
18. A. Ismael, N. T. M. Eldabe, M. Abouzeid, S. Elshabouri, Entropy generation and nanoparticles Cu O effects on MHD peristaltic transport of micropolar non-Newtonian fluid with velocity and temperature slip conditions, Egyptian Journal of Chemistry, 65 (2022) 715-722.
19. S. Nadeem, S. Akram, Magnetohydrodynamic peristaltic flow of a hyperbolic tangent fluid in a vertical asymmetric channel with heat transfer. Acta Mechanica Sinica, **27**(2), 237-250, (2011).
20. S. Nadeem and S. Akram, Peristaltic Transport of a Hyperbolic Tangent Fluid Model in an Asymmetric Channel. Zeitschrift für Naturforschung A, **64**(a), 559-567, (2009).
21. T. Hayat, N. Aslam, A. Alsaedi, M. Rafiq, Endoscopic effect in MHD peristaltic activity of hyperbolic tangent nanofluid: A numerical study. International Journal of Heat and Mass Transfer, **115**, 1033–1042, (2017).
22. T. Hayat, M. Shafique, A. Tanveer and A. Alsaedi A., Magnetohydrodynamic effects on peristaltic flow of hyperbolic tangent nanofluid with slip conditions and Joule heating in an inclined channel. International Journal of Heat and Mass Transfer, **102**, 5–63, (2016).
23. M.Y. Abou-zeid, Homotopy perturbation method for couple stresses effect on MHD peristaltic flow of a non-Newtonian nanofluid.

Microsystem Technologies, **24**, 4839–4846, (2018).

24. A. Alsaedi, N. Ali, D. Tripathi and T. Hayat, Peristaltic flow of couple stress fluid through uniform porous medium. Applied Mathematics and Mechanics - English Edition, **35**, 469–480, (2014).
25. A.M. Ismael, N. T. Eldabe, M. Y. Abou-zeid, S. M. Elshabouri, Thermal micropolar and couple stresses effects on peristaltic flow of biviscosity nanofluid through a porous medium. Science Reports, **12**,16180 (2022).
26. A.J. Abuiyada, N.T. Eldabe, M.Y. Abouzeid, S. Elshabouri, Effects of thermal diffusion and diffusion thermo on a chemically reacting MHD peristaltic transport of Bingham plastic nanofluid. Journal of advanced research in fluid mechanics and thermal science, **98** (2), 24-43 (2022).
27. N.T. El-dabe, A.A. Shaaban, M.Y. Abou-Zeid, and H.A. Ali, Magnetohydrodynamic non-Newtonian nanofluid flow over a stretching sheet through a non-Darcy porous medium with radiation and chemical reaction. Journal of Computational and Theoretical Nanoscience, **12**, 5363–5371, (2015).
28. M.Y. Abou-zeid, Homotopy perturbation method for MHD non-Newtonian nanofluid flow through a porous medium in eccentric annuli in peristalsis. Thermal Science, **5**, 2069-2080 (2017).
29. M.Y. Abou-zeid, M.A.A. Mohamed, Homotopy perturbation method for creeping flow of non-Newtonian power-law nanofluid in a nonuniform inclined channel with peristalsis. Zeitschrift für Naturforsch A **72**, 899–907, (2017).
30. N.T.M. Eldabe, M.Y. Abou-zeid, M.A.A. Mohamed and M. M. Abd-Elmoneim, MHD peristaltic flow of non-Newtonian power-law nanofluid through a non-Darcy porous medium inside a non-uniform inclined channel, Archive of Applied Mechanics, **91**, 1067–1077, (2021).
31. M.El. Ouaf and M. Abou-zeid, Electromagnetic and non-Darcian effects on a micropolar non-Newtonian fluid boundary-layer flow with heat and mass transfer. International Journal of Applied Electromagnetics and Mechanics. **66**, 693-703, (2021).
32. M.Y. Abou-zeid, A. A. Shaaban, and M. Y. Alnour, Numerical treatment and global error estimation of natural convective effects on gliding motion of bacteria on a power-law nanoslime through a non-Darcy porous medium. Journal of Porous Media, **18**, 1091–1106, (2015).
33. M.El.M. Ouaf, and M.Y. Abou-zeid, Hall currents effect on squeezing flow of non-Newtonian nanofluid through a porous medium between two parallel plates, Case Studies in Thermal Engineering, **28**, 101362, (2021).
34. Mostafa, Y., El-Dabe, N., Abou-Zeid, M., Ouaf, M., Mostapha, D.: Peristaltic Transport of Carreau Coupled Stress Nanofluid with Cattaneo-Christov Heat Flux Model Inside a Symmetric Channel. J. Adv. Res. Fluid Mech. Therm. Sci. 98(1), 1-17 (2022)
35. N.T.M. Eldabe, M.Y. Abouzeid, and H.A. Shawky, MHD peristaltic transport of Bingham blood fluid with heat and mass transfer through a non-uniform channel, Journal of advanced research in fluid mechanics and thermal science, **77** (2), 145-159, (2021).
36. N.T.M. Eldabe, R.R. Rizkallah, M.Y. Abou-zeid, and V.M. Ayad, Effect of induced magnetic field on non-Newtonian nanofluid Al2IO3 motion through boundary-layer with gyrotactic microorganisms. Thermal Science, **26**, 411 – 422, (2022).
37. Kh. Nowar, Peristaltic Flow of a Nanofluid under the Effect of Hall Current and Porous Medium. Mathematical Problems in Engineering, **2014**, ID: 389581, (2014).
38. E. Abo-Eldahab, E. Barakat, and Kh. Nowar, Hall Currents and Heat Transfer Effects on Peristaltic Transport in a Vertical Asymmetric Channel through a Porous Medium. Mathematical Problems in Engineering, **2012**, 840203, (2012).
39. J.F. Schmidt, Effect of Magnetic field on the conduction heat transfer at the stagnation point of a partially ionized argon gas. National Aeronautics and Space Administration, Washington, (1996).
40. S. Rashidi, J.A. Esfahani and M. Maskaniyan, "Applications of magnetohydrodynamics in biological systems-A review on the numerical studies. Journal of Magnetism and Magnetic

Materials, (2017), doi: http://dx.doi.org/10.1016/j.jmmm.2017.05.014.

41. M.Y. Abouzeid, Chemical reaction and non-Darcian effects on MHD generalized Newtonian nanofluid motion, Egyptian Journal of Chemistry, **65**(12), 647-655, (2022).
42. M.Y. Abou-zeid, Implicit homotopy perturbation method for MHD non-Newtonian nanofluid flow with Cattaneo-Christov heat flux due to parallel rotating disks, Journal of nanofluids 8(8), 1648-1653, (2019).
43. N.T. El-Dabe, M.Y. Abouzeid, and O.S. Ahmed, Motion of a thin film of a fourth grade nanofluid with heat transfer down a vertical cylinder: Homotopy perturbation method application, Journal of Advanced Research in Fluid Mechanics and Thermal Sciences, **66** (2), 101-113, (2020).
44. M.Y. Abou-zeid, Homotopy perturbation method to gliding motion of bacteria on a layer of power-law nanoslime with heat transfer. Journal of Computational and Journal of Computational and Theoretical Nanoscience, **12**, 12:3605-3614, (2015).
45. N.T.M. Eldabe, G.M. Moatimid, M. Abou-zeid, A.A. Elshekhipy, and N.F. Abdallah, Instantaneous thermal-diffusion and diffusion-thermo effects on carreau nanofluid flow over a stretching porous sheet. Journal of Advanced Research in Fluid Mechanics and Thermal Sciences, **72**(2), 142-157, (2020).
46. M.G. Ibrahim, and M.Y. Abou-zeid, Influence of variable velocity slip condition and activation energy on MHD peristaltic flow of Prandtl nanofluid through a non-uniform channel. Science Reports, **12**,18747, (2022).
47. N.T. Eldabe, M.Y. Abou-zeid, O.H. El-Kalaawy, S.M. Moawad, and O.S Ahmed, Electromagnetic steady motion of Casson fluid with heat and mass transfer through porous medium past a shrinking surface, Thermal Science, **25**(1A), 257-265, (2021).
48. N.T.M. Eldabe, R.R. Rizkallah, M.Y. Abou-zeid, and V.M. Ayad, Thermal diffusion and diffusion thermo effects of Eyring- Powell nanofluid flow with gyrotactic microorganisms through the boundary layer, Heat Transfer - Asian Research, **49**, 383 – 405, (2020).
49. M.Y. Abou-zeid, Magnetohydrodynamic boundary layer heat transfer to a stretching sheet including viscous dissipation and internal heat generation in a porous medium, Journal of Porous Media, **14**, 1007-1018, (2011).
50. H.M. Mansour, M.Y. Abou-zeid, Heat and mass transfer effect on non-Newtonian fluid flow in a non-uniform vertical tube with peristalsis. Journal of advanced research in fluid mechanics and thermal science, **61**(1), 44–62 (2019).
51. N.T.M. Eldabe, M.Y. Abou-zeid, A. Abosaliem, A. Alana, and N. Hegazy, Thermal Diffusion and Diffusion Thermo Effects on Magnetohydrodynamics Transport of Non-Newtonian Nanofluid Through a Porous Media Between Two Wavy Co-Axial Tubes. IEEE Transactions on Plasma Science, **50**, 1282-1290, (2021).
52. W. Abbas, N. T. M. Eldabe, R. A. Abdelkhalek, N. A. Zidan, and S.Y.Marzouk, Soret and Dufour Effects with Hall Currents on Peristaltic Flow of Casson Fluid with Heat and Mass Transfer Through Non-Darcy Porous Medium Inside Vertical Channel. Egyptian Journal of Chemistry, **64**(9), 5215 – 5225, (2021).
53. N. Hegazy, N.T. Eldabe, M.Y. Abouzeid, A. Abousaleem, and A. Alana, Influence of both chemical reaction and electro-osmosis on MHD non-Newtonian fluid flow with gold nanoparticles. Egyptian Journal of Chemistry, 66 (2023). 191-201.
54. M. Ouaf, M. Abouzeid, and M.G.Ibrahim, Effects of both variable electrical conductivity and microstructural/multiple slips on MHD flow of micropolar nanofluid. Egyptian Journal of Chemistry, 66 (2023). 449-456.
55. L.H. Alwan, and L.A. AL JEBUR, Studying the effect of gold nanoparticles on mixture of surfactant of sodium dodecyl benzene sulfonate (SDBS) surfactant and folic acid. Egyptian Journal of Chemistry, **65** (3), 358-394, (2022).
56. Abuiyada, A. Eldabe, N. T., Abouzeid, M. Y. Elshabouri, S. Influence of both Ohmic dissipation and activation energy on peristaltic transport of Jeffery nanofluid through a porous media, CFD Letters 15, Issue 6 (2023) 65-85.
57. O. S. Ahmed, N. T. Eldabe, M. Y. Abou-zeid, O. H. El-kalaawy and S. M. Moawad, Numerical treatment and global error estimation for thermal electro-osmosis effect on non-Newtonian

nanofluid flow with time periodic variations, Sci. Rep. 13 (2023) 14788.
58. H. A. Sayed and M. Y. Abouzeid, Radially varying viscosity and entropy generation effect on the Newtonian nanofluid flow between two co-axial tubes with peristalsis. Scientific Reports 13 (2023), 11013.
59. M. G. brahim and M. Y. Abouzeid, Computational simulation for MHD peristaltic transport of Jeffrey fluid with density-dependent parameters. Scientific Reports 13 (2023), 9191.
60. M. G. brahim and M. Y. Abouzeid, Computational simulation for MHD peristaltic transport of Jeffrey fluid with density-dependent parameters. Scientific Reports 13 (2023), 9191.
61. Mohamed, Y. M., Eldabe, N. T., Abou-zeid, M. Y., Mostapha, D. R. & ouaf, M. E., Impacts of chemical reaction and electric field with Cattaneo - Christov theories on peristaltic transport of a hyperbolic micropolar nanofluid, Egyptian Journal of Chemistry, 66 (7) (2023) 63 – 85.
62. Mohamed, Y. M., Eldabe, N. T., Abou-zeid, M. Y., Ouaf, M. E. & Mostapha, D. R., Chemical reaction and thermal radiation via Cattaneo-Christov double diffusion (ccdd) effects on squeezing non-Netonian nanofluid flow between two - parallel plates, Egyptian Journal of Chemistry, 66 (3) (2023) 209 – 231.
63. Abdelmoneim, M., Eldabe, N.T., Abouzeid, M.Y., Ouaf, M.E.: Both modified Darcy's law and couple stresses effects on electro-osmotic flow of non-Newtonian nanofluid with peristalsis. Int. J. Appl. Electromagn. Mech. 72(3), 253–277 (2023).
64. Eldabe, N. T., Abouzeid, M. Y. Mohamed, M. A. A., Abd-Elmoneim, M. M. Peristaltic mixed convection slip flow of a Bingham nanofluid through a non-darcy porous medium in an inclined non-uniform duct with viscous dissipation and radiation. J. Appl. Nonlinear Dyn. 12, 231-243 (2023).
65. Eldabe, N.T., Abou-Zeid, M.Y. The wall properties effect on peristaltic transport of micropolar non-newtonian fluid with heat and mass transfer, Mathematical Problems in Engineering, 808062 (2010).
66. Eldabe, N.T., Abou-Zeid, M.Y. The wall properties effect on peristaltic transport of micropolar non-newtonian fluid with heat and mass transfer, Mathematical Problems in Engineering, 808062 (2010).
67. Shaaban, A.A., Abou-Zeid, M.Y. Effects of heat and mass transfer on MHD peristaltic flow of a non-newtonian fluid through a porous medium between two co-axial cylinders, Mathematical Problems in Engineering, 819683 (2013).